



Computational prediction of salt and cocrystal structures—Does a proton position matter?

Sharmarke Mohamed, Derek A. Tocher, Sarah L. Price*

Department of Chemistry, University College London, 20 Gordon Street, London WC1H 0AJ, UK

ARTICLE INFO

Article history:

Received 16 December 2010
Received in revised form 4 March 2011
Accepted 24 March 2011
Available online 8 April 2011

Keywords:

Crystallization
Salt
Cocrystal
Proton transfer
Crystal structure prediction

ABSTRACT

The lattice energy landscape is calculated for three pyridinium carboxylate salts and the corresponding pyridine-carboxylic acid cocrystals. Experimentally, one system crystallizes as a salt, another as a cocrystal and the acidic proton in the third is disordered across the $N_{\text{arom}} \cdots O$ hydrogen bond vector. A novel structure of a 1:1 4-cyanopyridine-4-fluorobenzoic acid cocrystal (**I**) was characterized to provide the cocrystal as a system with an isolated carboxylic acid–pyridine heterosynthon. By contrast, the 4-dimethylaminopyridinium maleate salt (**GUKVUE**) shows the effects of an internal hydrogen bond, and the proton-disordered pyridine-isophthalic acid crystal (**IYUPEX**) shows the effects of competing intermolecular hydrogen bonds. All three crystal structures were found low in energy on the lattice energy landscape for the correct proton connectivity. For all three systems, comparing the salt and cocrystal energy landscapes shows the importance of the proton position for the relative stabilities of structures, despite the expected similarities between the ionized and neutral forms of the carboxylic acid–pyridine heterosynthon. The systems with additional hydrogen bonds have some hydrogen bonding motifs that are only favourable for the salt or for the cocrystal. This illustrates the sensitivity of the range of thermodynamically plausible crystal structures to whether the molecules are assumed to be ionized or neutral.

© 2011 Elsevier B.V. All rights reserved.

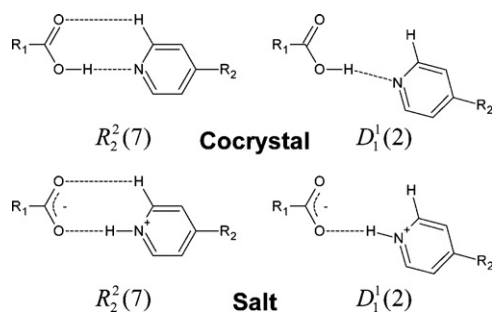
1. Introduction

The potential for a computational method of predicting polymorphs has long been recognized as potentially important for the pharmaceutical industry (Price, 2004; Verwer and Leusen, 1998). There have been significant advances in our ability to calculate realistic crystal energy landscapes, the set of crystal structures which are thermodynamically feasible, for single component systems. Comparison with academic polymorph screening and characterization studies is revealing how these should be interpreted as an aid to polymorph screening (Braun et al., 2011; Price, 2009). However, generating lattice energy landscapes for multi-component systems, such as salts, cocrystals and solvates, is intrinsically more difficult because the additional variables describing the relative orientation of the two components adds more dimensions to the search for possible structures. This problem is being overcome by adaptation of methods and increased computer speeds, and insights into the crystallization of solvates and cocrystals have recently been derived from multi-component lattice energy landscapes (Cruz-Cabeza et al., 2006, 2008; Day et al., 2009; Habgood et al., 2010; Habgood and Price, 2010; Karamertzanis et al., 2007; Polito et al.,

2008). There is an additional issue for the prediction of salts in that the models for the lattice energy have been developed for neutral molecules and these may not be sufficiently accurate when transferred to salts. There have been some successful studies of certain diastereomeric salts using atomistic modelling (Karamertzanis et al., 2007) and pyridinium chloride using dispersion-corrected density functional methods (van de Streek et al., 2010).

Many carboxylic acids are widely used in pharmaceutical salts and cocrystals. When the pK_a difference between the acid and conjugate acid of the base is in the range 0–3 (Childs et al., 2007) crystallization may result in a salt, cocrystal or disordered solid form with partial proton transfer (Bhogala et al., 2005; Childs et al., 2007; Johnson and Rumon, 2008). Under some circumstances, it may be difficult to determine whether a salt or cocrystal has been obtained (Stevens et al., 2010b) prior to obtaining sufficient quality single crystals for X-ray diffraction work. The carboxylic acid–pyridine synthon, widely used in the supramolecular synthesis of cocrystals (Almarsson and Zaworotko, 2004; Bhogala et al., 2005), illustrates (Scheme 1) the similarity between the salt and cocrystal form (Shattock et al., 2008). The contribution of the proton to the packing is insignificant, and hence we would expect that the densely packed crystal structures would be very similar for the salt and cocrystal. The generation of plausible crystal structures and testing of crystal structure prediction methods requires fully determined crystal structures of rigid systems that have been

* Corresponding author. Tel.: +44 020 7679 4622; fax: +44 020 7679 7463.
E-mail address: s.l.price@ucl.ac.uk (S.L. Price).



Scheme 1. The neutral, $\text{COOH}\cdots\text{N}_{\text{arom}}$, and ionized, $\text{COO}^-\cdots\text{H-N}_{\text{arom}}^+$, forms of the carboxylic acid–pyridine heterosynthons depicted using the $R_2^2(7)$ or $D_1^1(2)$ graph sets (Etter et al., 1990). The $\text{C-O}\cdots\text{N}_{\text{arom}}\text{-C}$ or $\text{C-O}\cdots\text{N}_{\text{arom}}\text{-C}$ torsion angle is $\leq 15^\circ$ in the $R_2^2(7)$ and $>15^\circ$ in the $D_1^1(2)$ motifs.

screened for polymorphism. Our previous study (Mohamed et al., 2009) characterizes a salt suitable for calculating both salt and cocrystal lattice energy landscapes, 4-dimethylaminopyridinium maleate (**GUKVUE**). This study also confirmed the absence of polymorphs on crystallizing pyridine with isophthalic acid, which gives a suitable disordered salt:cocrystal system, pyridine-isophthalic acid:pyridinium isophthalate (58%:42%; **IYUPEX**) (Dale et al., 2004). To provide a suitable 1:1 cocrystal for this study, we perform a screen for a cocrystal of 4-cyanopyridine and 4-fluorobenzoic acid, and characterize its crystal structure. These *para*-substitutions of benzoic acid and pyridine would provide an example of a carboxylic acid–pyridine heterosynthons with minimal competing intermolecular interactions, and a cocrystal should be formed because the ΔpK_a is -2.29 (4-cyanopyridine $\text{pK}_a = 1.86$ (Fischer et al., 1964),

4-fluorobenzoic acid $\text{pK}_a = 4.15$ (Albert and Serjeant, 1984) under aqueous conditions).

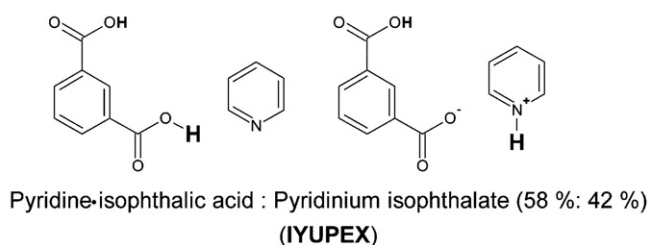
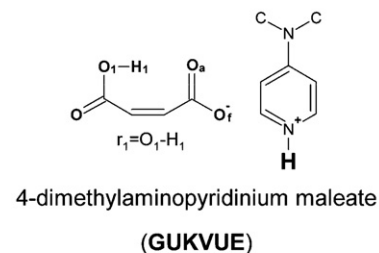
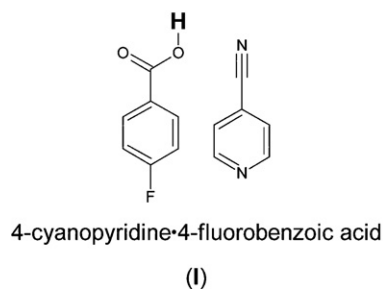
This paper uses a simple, relatively computationally inexpensive form of multi-component (1:1 stoichiometry) crystal structure prediction to see whether it can predict the crystal structure of a salt, cocrystal and a disordered salt:cocrystal system. The computational method is based on using the structures and charge distributions of the ions or molecules in isolation, calculated *ab initio*, and assuming that these remain the same in the crystal. The ability to predict such multi-component crystals is tested by calculating the lattice energy landscape of 4-cyanopyridine-4-fluorobenzoic acid, 4-dimethylaminopyridinium maleate and pyridine-isophthalic acid (Scheme 2). The crystal structure prediction is then repeated using the molecular model that would be obtained after acid–base proton transfer (Scheme 2) so as to determine the sensitivity of the predictions to the covalent bonding of the acidic proton. Thus, this study calculates approximate lattice energy landscapes for the three salts and three cocrystals shown in Scheme 2 and tests their ability to predict the salt, cocrystal and disordered system found experimentally, with the observed or alternative acidic proton assignment.

2. Materials and methods

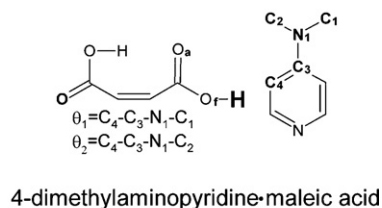
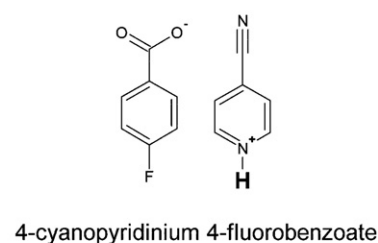
2.1. Experimental screen for a cocrystal of 4-cyanopyridine and 4-fluorobenzoic acid

Commercial samples of 4-cyanopyridine (Alfa Aesar, 98% purity) and 4-fluorobenzoic acid (Sigma–Aldrich, 98% purity) were used

Experimental molecular structures



Hypothetical molecular structures



Scheme 2. Experimental molecular structures of the pure cocrystal, pure salt, and disordered salt:cocrystal and the hypothetical molecular structures expected following transfer of the acidic proton in bold type. The observed crystal structure is indicated by parenthesis. The bond lengths and torsion angles (r_1 , θ_1 and θ_2) that were constrained to experimental neutron/X-ray diffraction values during *ab initio* geometry optimization are marked. O_a (acceptor) and O_f (free) distinguish the oxygen atoms on maleic acid. Non-polar hydrogen atoms are omitted for clarity.

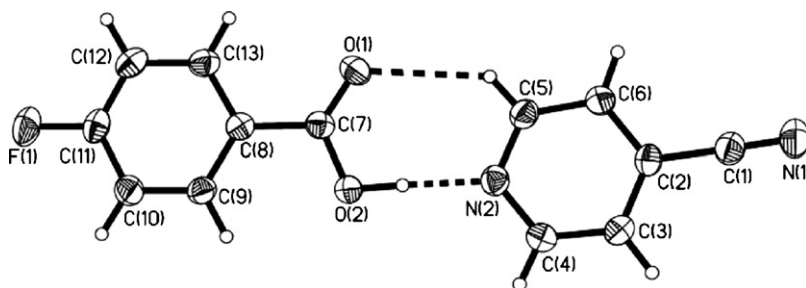


Fig. 1. The asymmetric unit of the 4-cyanopyridine-4-fluorobenzoic acid (1:1) cocrystal, **I**. Displacement ellipsoids are drawn at the 50% probability level and hydrogen atoms are shown as spheres of arbitrary radius.

without further purification. Solution experiments were performed by lightly grinding (pestle and mortar) a stoichiometric 1:1 molar ratio of 4-cyanopyridine and 4-fluorobenzoic acid and dissolving the resulting powder in the minimum amount of solvent needed to dissolve 0.1 g of solute. The solvents screened were methanol, ethanol, acetone, tetrahydrofuran and water. In all cases, the solutions were filtered to remove any excess solute particles and the solvent was allowed to evaporate at the temperatures -4 , 5 and 25 °C. The extent of the solution screening was necessarily limited to solvents with reasonably similar solubilities of the acid and base. Grinding experiments (Friscic and Jones, 2009; Karki et al., 2007) were performed using a *Retsch MM200* mixer mill, equipped with 10 mL capacity stainless steel grinding jars and two 5 mm stainless steel grinding balls per jar. A stoichiometric 1:1 molar ratio of 4-cyanopyridine and 4-fluorobenzoic acid was used in neat grinding and solvent drop grinding experiments. In all cases, the combined mass of solute in the grinding jar did not exceed 0.5 g. Solvent drop grinding experiments were performed by adding 4 drops of solvent to the stoichiometric mixture of acid and base. Neat grinding experiments were performed at a frequency of 30 Hz for 60 min while solvent drop grinding experiments were performed at the same frequency but for 30 min. A PerkinElmer Spectrum One Fourier Transform-Infrared (FT-IR) spectrometer was used to characterize the ground samples. For each sample, spectra were collected at a resolution of 4 cm^{-1} using 15 scans in the wavenumber range $650\text{--}4000\text{ cm}^{-1}$.

2.2. Single crystal X-ray diffraction

Single crystal X-ray diffraction experiments were performed on a Bruker AXS SMART APEX CCD diffractometer equipped with a Bruker AXS Kryoflex open flow cryostat (graphite monochromated Mo- K_{α} radiation, $\lambda = 0.71073\text{ \AA}$). Data integration and final unit cell parameters were obtained via SAINT+ (Bruker AXS Inc., 2003).

The absorption correction was performed via a semi-empirical approach using SADABS (Sheldrick, 2001), and the crystal structure of **I** was solved by direct methods using SHELXS-97 (Sheldrick, 1997b). All atoms were located from the difference Fourier map. For the non-hydrogen atoms, an anisotropic model was used for the thermal parameters and the atomic co-ordinates freely refined. All hydrogen atom co-ordinates and isotropic thermal parameters were also freely refined. The SHELXL-97 (Sheldrick, 1997a) package was used for structure refinement. Packing diagrams were produced using Mercury CSD 2.2 (Macrae et al., 2006).

2.3. Computational modelling

Ab initio geometry optimizations of all the molecules and ions in Scheme 2 were performed at the MP2/6-31G(d,p) level of theory using GAUSSIAN03 (Frisch et al., 2003). This immediately showed the limitations of assuming that the covalent bonding remains the same in the gas and crystal phases, as the unconstrained minima had a pyramidal nitrogen amine in 4-dimethylaminopyridine and the intramolecular proton was between the two oxygen atoms in the maleate ion, which are not found in crystal structures. Hence, the maleate O–H bond length was constrained to the standard neutron (Allen et al., 1987) value of 1.015 \AA and the dihedral angles defining the methyl groups of 4-dimethylaminopyridine were constrained to the experimental values to give a near planar geometry at nitrogen in the *ab initio* optimizations of their molecular structures. The *ab initio* charge densities were also used to provide a model for the electrostatic contribution to the lattice energies: the potential derived atomic charges (Breneman and Wiberg, 1990) were used in the CrystalPredictor search and the atomic multipoles, derived by a distributed multipole analysis (Stone, 2005) using GDMA2.2, were used in the final lattice energies.

The lattice energy landscapes for the six systems shown in Scheme 2 were generated keeping the *ab initio* optimized

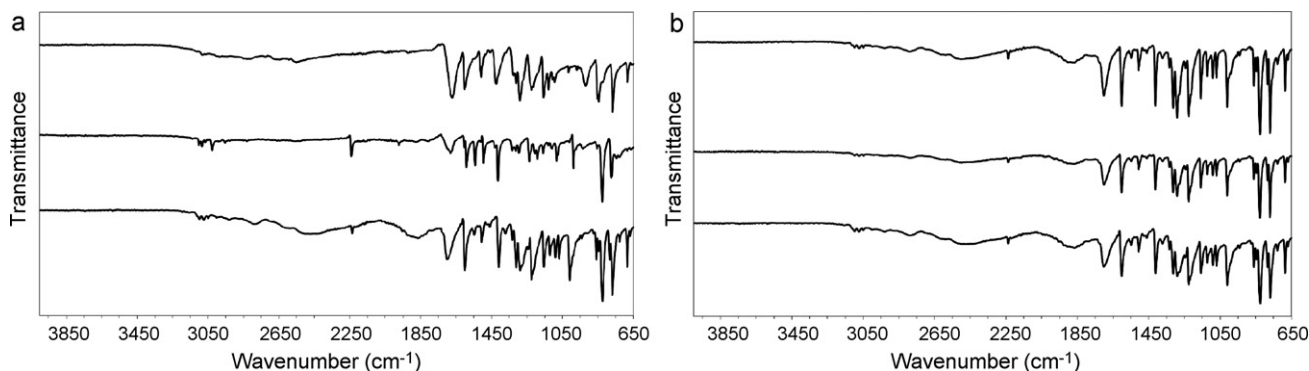


Fig. 2. (a) Comparison of the characteristic FT-IR spectra of 4-fluorobenzoic acid (top) and 4-cyanopyridine (middle) starting reagents with the spectrum of **I** (bottom). (b) The results of neat grinding over 60 min (top) and solvent drop grinding using methanol over 30 min (middle) produce the cocrystal, **I**, obtained from the solution crystallization experiments (bottom). Solvent drop grinding with ethanol, acetone and tetrahydrofuran produced samples with the same spectrum as shown for methanol.

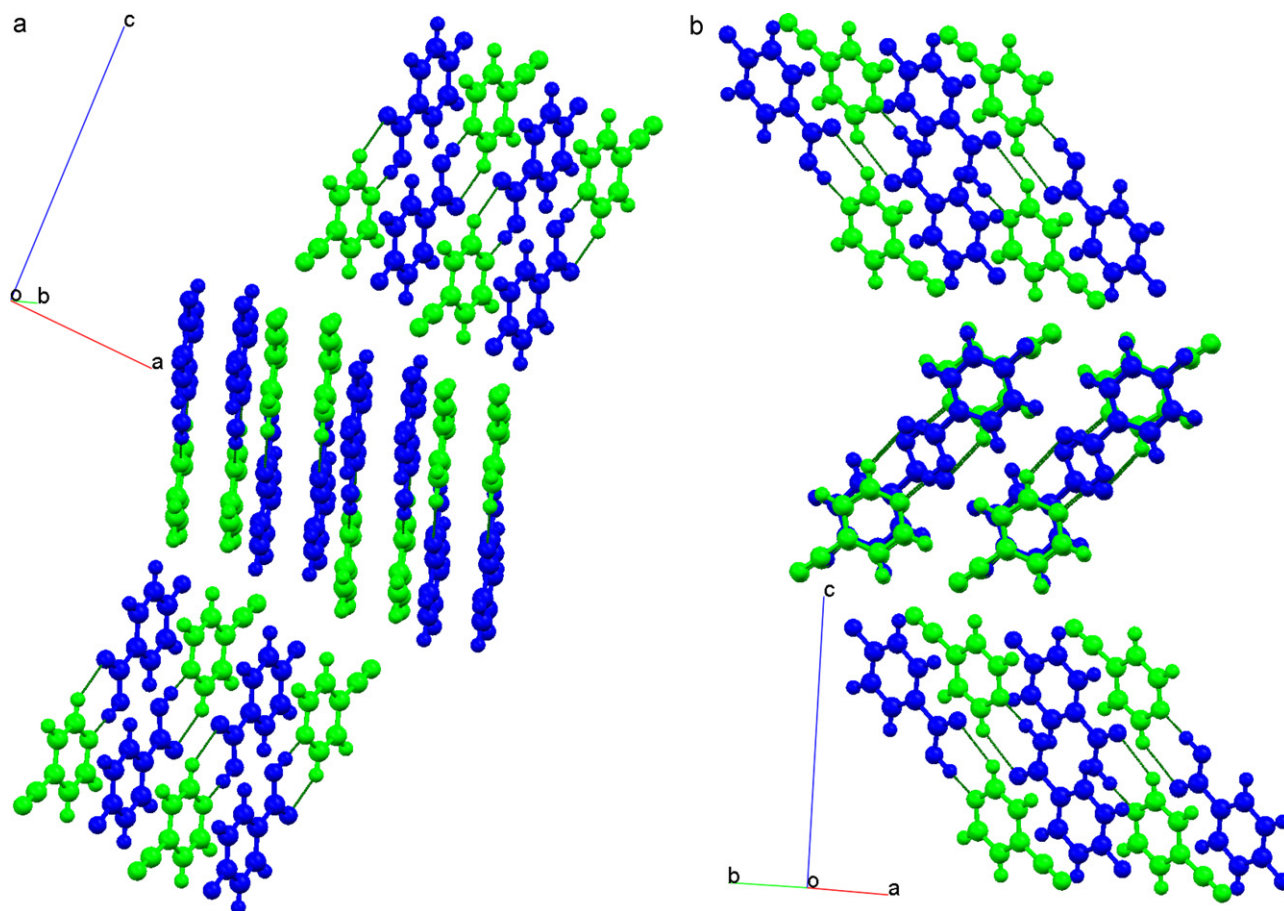


Fig. 3. Alternative views of the crystal packing for the 4-cyanopyridine-4-fluorobenzoic acid cocrystal, I. (a) The molecular heterodimers between 4-fluorobenzoic acid (blue) and 4-cyanopyridine (green) in I. The packing is such that the heterodimers do not form two-dimensional sheets. (b) The π - π stacking (centroid-centroid separation 3.78 Å) between acid and base molecules of inversion related dimers viewed perpendicular to the central layer. (For interpretation of the references to color in this figure legend, the reader is referred to the web version of this article.)

molecule/ion rigid throughout. CrystalPredictor (Karamertzanis and Pantelides, 2005) was used to generate hypothetical cocrystal or salt structures in the space groups $P\bar{1}$, $P2_1$, $P2_1/c$, $P2_12_12$, $P2_12_12_1$, $Pna2_1$, $Pca2_1$, $Pbca$, $Pbcn$, Cc , $C2$, $C2/c$, $P2_1/m$ and $C2/m$. These were lattice energy minimized using the atomic charges and an atom-atom $exp-6$ model for the repulsion-dispersion contributions. The potential parameters had been empirically fitted to related crystal structures for C, H_C, N (Williams and Cox, 1984), O (Cox et al., 1981), F (Williams and Houpt, 1986), and the polar protons, H_N (Coombes et al., 1996) and H_O (Beyer and Price, 2000), and have been extensively tested in conjunction with distributed multipole electrostatic models for neutral molecules (Price et al., 2010). Following the CrystalPredictor searches, the 1000 lowest energy structures produced were passed to DMACRYS (Price et al., 2010) for rigid body lattice energy minimizations using the more accurate distributed multipole electrostatic model. These structures were clustered to remove duplicate crystal structures and the second derivative matrix examined to ensure all structures were true lattice energy minima.

Crystal structures were compared using the best overlay of the 15-molecule co-ordination sphere as calculated using the Crystal Packing Similarity Analysis (Chisholm and Motherwell, 2005) in Mercury CSD 2.3 (Macrae et al., 2008). The calculated root-mean-square deviation of the intermolecular atom-atom distances (RMSD₁₅) ignores hydrogen atoms, and the 15 molecules are only considered to match if all the intermolecular atom-atom distances agree within 30% and angles within 30° between the two structures. This is a significantly less strict criterion for match-

ing than the default limits of 20% and 20°. The hydrogen bond motifs and associated graph sets of the predicted crystal structures within 10 kJ mol⁻¹ of the global minimum were also calculated with the Molecular Materials Studio feature of Mercury CSD 2.3. The $R_2^2(7)$ and $D_1^1(2)$ acid-base/anion-cation interaction motifs were distinguished (Sarma et al., 2009) by the C-O \cdots N_{arom}⁺-C or C-O \cdots N_{arom}-C torsion angle (Scheme 1). This angle is less than or equal to 15° for an $R_2^2(7)$ motif and the two molecules/ions are approximately coplanar, whereas if the torsion angle is greater than 15°, the motif is designated $D_1^1(2)$. The intramolecular hydrogen bond in the maleate anion produces a significant asymmetry between the two carboxylate oxygen atoms, and so we denote the motif type O_f when the intermolecular hydrogen bond is to the oxygen not involved in the intramolecular hydrogen bond and type O_a when the same oxygen is involved in the inter and intramolecular hydrogen bonds. Isophthalic acid is a 1,3-dicarboxylic acid that can participate in intermolecular hydrogen bonding for both acidic functional groups. Thus the salt and cocrystal structures of isophthalic acid were analyzed in terms of the combined acid-base/anion-cation and acid-acid/anion-anion hydrogen bonding motifs.

The structures on the salt and cocrystal landscapes could be compared in the same way, using the packing similarity feature of Mercury CSD 2.3. Visual inspection of the acid-base/anion-cation hydrogen bond motif was also performed for all salt-cocrystal pairs. The resulting re-ranking of the relative lattice energies of different salt or cocrystal structures was confirmed by also re-positioning the acidic proton in each low energy salt structure to give a cocrys-

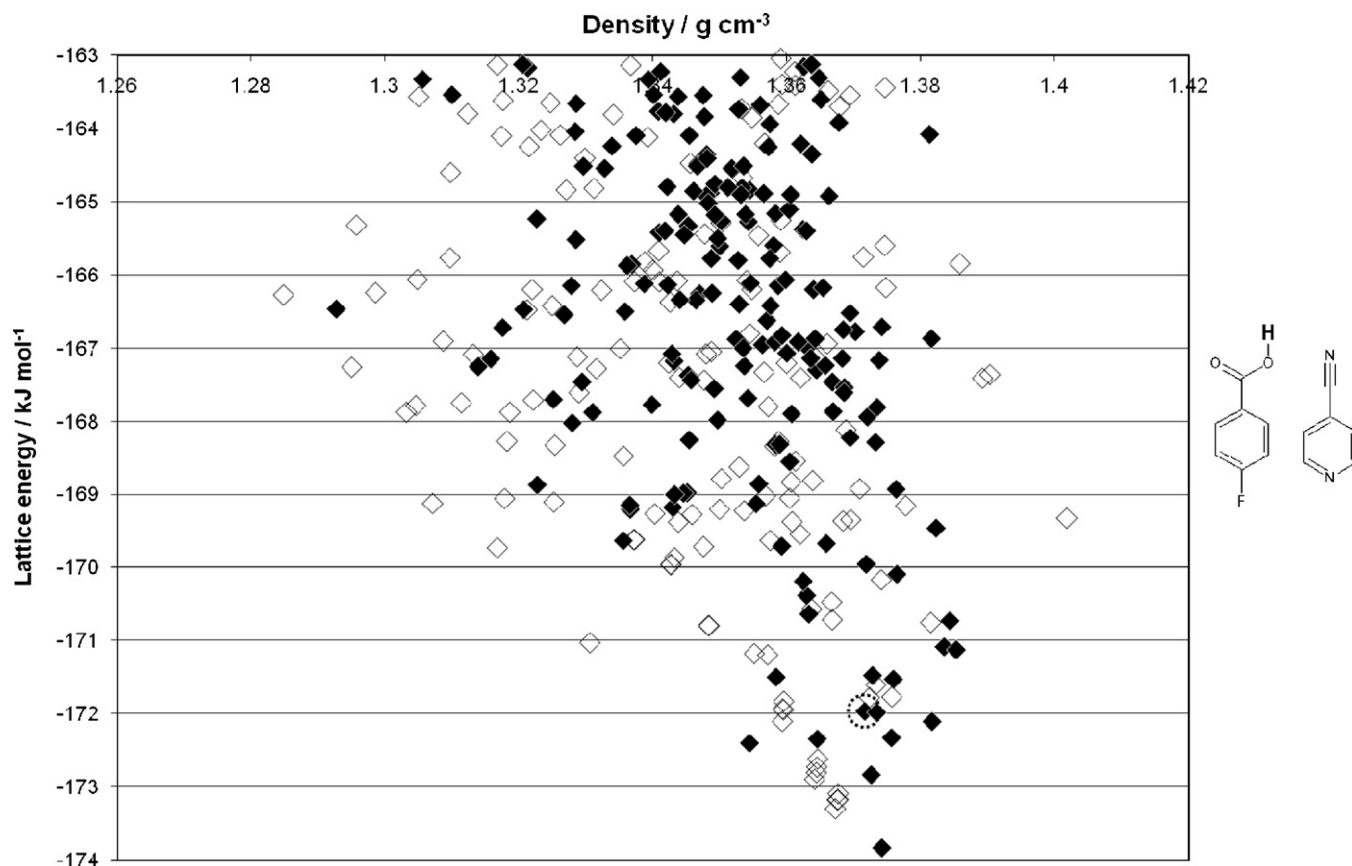


Fig. 4. Lattice energy landscape of the 4-cyanopyridine-4-fluorobenzoic acid cocrystal, with each point representing a crystal structure, classified by the graph set of the hydrogen bond motif. Solid diamonds denote the $R_2^2(7)$ motif and open diamonds denote the $D_1^1(2)$ motif. The large dotted circle denotes the lattice energy minimum corresponding to the experimental structure (I).

tal. Mercury CSD 2.3 was used to edit the salt structure to give the desired O–H acid geometry, and the lattice energy of the resulting cocrystal structure was then minimized using the same conformation and multipole model used in the cocrystal search.

3. Results

3.1. Crystal structure of 4-cyanopyridine-4-fluorobenzoic acid (1:1)

Solution crystallizations of a 1:1 molar ratio of 4-cyanopyridine and 4-fluorobenzoic acid in methanol, ethanol, acetone and tetrahydrofuran all led to block-like crystals of a 4-cyanopyridine-4-fluorobenzoic acid cocrystal, **I**, with a 1:1 stoichiometry (Fig. 1). The products identified after neat grinding and solvent drop grinding were the same and corresponded to the 1:1 cocrystal. Characteristic vibrational bands that led to this identification include the nitrile stretching vibration (Fig. 2) which has a characteristic absorption in the wavenumber range 2200–2300 cm^{-1} .

The 4-cyanopyridine-4-fluorobenzoic acid cocrystal, **I**, crystallizes in the monoclinic space group $C2/c$. The C–O...N_{arom}–C torsion of 1.15° shows it has formed a near idealized acid–base hydrogen bond motif with the graph set $R_2^2(7)$. Other close contacts are between the C3 proton and the F and cyanide nitrogen, determining the relative orientation of the stacks of the acid–base hydrogen bonded pairs (Fig. 3). The salt structure **GUKVUE** is similar to the cocrystal in having an approximately planar $R_2^2(7)$ hydrogen bonded heterodimer (C–O...N_{arom}⁺–C torsion of 3.06°), with the intermolecular hydrogen bond to O_f. In the disordered crys-

tal, **IYUPEX**, the torsion angle is 27.11° and so the disordered C–O...H...N_{arom} hydrogen bond is classified as $D_1^1(2)$. Thus the series of three systems (c.f. Scheme 2) has one example of a near idealized isolated acid–base heterodimer synthon (**I**), another where an intramolecular hydrogen bond removes the pseudo-symmetry of the carboxylate group (**GUKVUE**), and a third where there are competing hydrogen bonding motifs (**IYUPEX**).

3.2. Lattice energy landscapes for 1:1 salts and cocrystals

3.2.1. 4-Cyanopyridine-4-fluorobenzoic acid (1:1) cocrystal

The calculated lattice energy landscape of the 4-cyanopyridine-4-fluorobenzoic acid cocrystal (Fig. 4) has the experimental cocrystal structure amongst the most stable structures, less than 2 kJ mol^{-1} above the global minimum structure. There are a wide range of different ways of packing the two molecules in the cocrystal with similar energies; all have an N_{arom}–H...O hydrogen bond, but in some the molecules are approximately coplanar, $R_2^2(7)$, and in others the C–O...N_{arom}–C torsion is more than 15° (i.e. $D_1^1(2)$). There are far fewer packings of the equivalent ions within 10 kJ mol^{-1} of the global minimum in the salt energy landscape (Fig. 5), but again both the $R_2^2(7)$ and $D_1^1(2)$ motifs are competitive in energy. The hypothetical 4-cyanopyridinium 4-fluorobenzoate salt structure derived from **I** is found 8.31 kJ mol^{-1} above the global minimum in the salt lattice energy landscape.

The salt and cocrystal energy landscapes have many structures in common (as judged by packing similarity comparisons). These related structures usually exhibit the same hydrogen bonding motif. However, the differences between the two energy land-

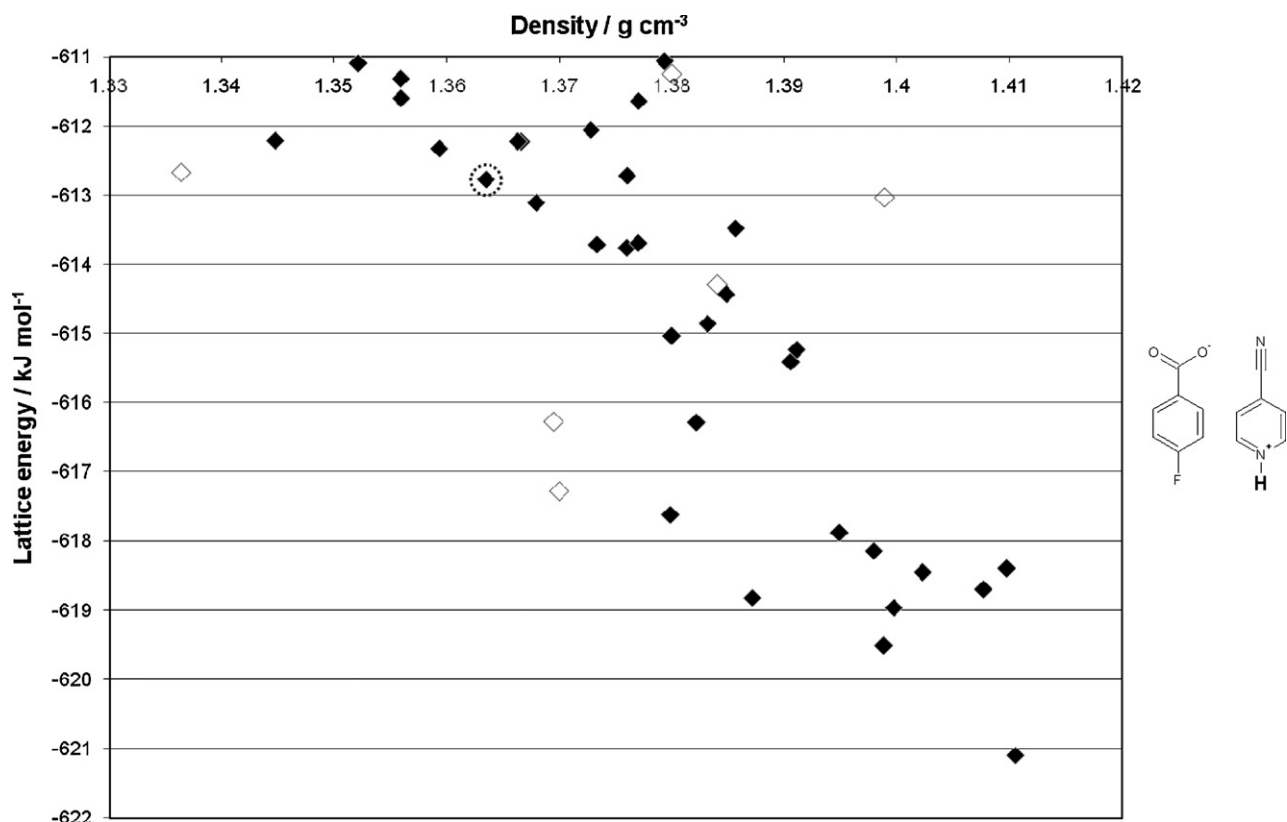


Fig. 5. Lattice energy landscape of the 4-cyanopyridinium 4-fluorobenzoate salt, with each point representing a crystal structure classified by the graph set of the hydrogen bond motif. Solid diamonds denote the $R_2^2(7)$ motif and open diamonds denote the $D_1^1(2)$ motif. The large dotted circle denotes the lattice energy minimum corresponding to the experimental structure (I) following repositioning of the hydrogen bonding proton.

scapes (Figs. 4 and 5) are far greater than a simple scaling of the energy axis reflecting the stronger ionic hydrogen bond. The correlation in the relative order of the lattice energies of corresponding salt cocrystal pairs was very poor. None of the salt structures within 5 kJ mol^{-1} of the global minimum corresponded to a favourable cocrystal (i.e. within 5 kJ mol^{-1} of the cocrystal global minimum).

The closest predicted cocrystal structure is a relatively poor match for the experimental structure with an RMSD_{15} of 0.466 \AA . This is also the case when modelled as a salt (RMSD_{15} of 0.416 \AA). Since the computed crystal structure has a significantly longer c axis than found experimentally (7% for cocrystal, 4% for salt model), this is due to poor modelling of the F and C \equiv N intermolecular contacts to CH bonds. This may also affect the relative lattice energies: cocrystal I is almost 10 kJ mol^{-1} more stable than the sum of the lattice energies of 4-cyanopyridine and 4-fluorobenzoic acid, which is relatively large compared with other estimates (Issa et al., 2009) of the thermodynamic stabilization of cocrystals. Poor modelling of these weaker intermolecular interactions may account for why there are a few other structures which are more stable than the observed cocrystal.¹

3.2.2. 4-Dimethylaminopyridinium maleate (1:1) salt

The calculated lattice energy landscape of 4-dimethylaminopyridinium maleate (Fig. 6) shows that the experimental structure of GUKVUE is predicted to be the most stable salt by a margin of 2 kJ mol^{-1} . Most of the other low energy salt struc-

tures are based on the alternative type $O_a R_2^2(7)$ motif, where the $N_{\text{arom}}^+ \cdots \text{H}$ donor forms a hydrogen bond to the carboxylate oxygen involved in the internal hydrogen bond (Fig. 7).

When the system is modelled as a cocrystal, the proton has to be transferred to O_f to give the observed conformation of maleic acid. All calculated cocrystal lattice energy minima maintain the $N_{\text{arom}} \cdots \text{H} \cdots O_f$ hydrogen bond which is observed for all three maleic acid cocrystals with aromatic nitrogen bases (GIPQAX, GANYEA and XEJXEQ) retrieved from the Cambridge Structural Database (Allen, 2002). The low energy cocrystal structures fall into two groups, with the $D_1^1(2)$ hydrogen bonded motif forming denser cocrystals of comparable stability to those based on the $R_2^2(7)$ heterodimer. The cocrystal equivalent of the experimental salt structure of GUKVUE is found 18th in stability in the lattice energy landscape of the hypothetical 4-dimethylaminopyridine-maleic acid cocrystal and is only 2.4 kJ mol^{-1} less stable than the most stable cocrystal structure generated in the search. The crystal packing is significantly less well reproduced when modelled as a cocrystal (Fig. 8). Thus the experimental salt structure, GUKVUE, is distinctive in adopting the hydrogen bond to O_f , which is characteristic of cocrystals of maleic acid. This structure has been correctly predicted as the most stable for this salt.

3.2.3. Pyridine-isophthalic acid:pyridinium isophthalate (58%:42%)

The calculated lattice energy landscapes of the 1:1 pyridine-isophthalic acid cocrystal (Fig. 9) and the 1:1 pyridinium isophthalate salt (Fig. 10) both contain a fully ordered version of the experimental structure IYUPEX which has the proton disordered such that there is a 58% contribution from the cocrystal and 42% from the salt. When modelled as a cocrystal, the crystal structure is well reproduced with a RMSD_{15} of 0.239 \AA , and

¹ The more stable structures which have the $R_2^2(7)$ motif match 5–11 molecules in the 15 molecule co-ordination sphere of I, and all the energetically competitive structures with the $D_1^1(2)$ motifs have a very similar coordination sphere. Hence there are far fewer structures that are possible competitive polymorphs than suggested by Fig. 4.

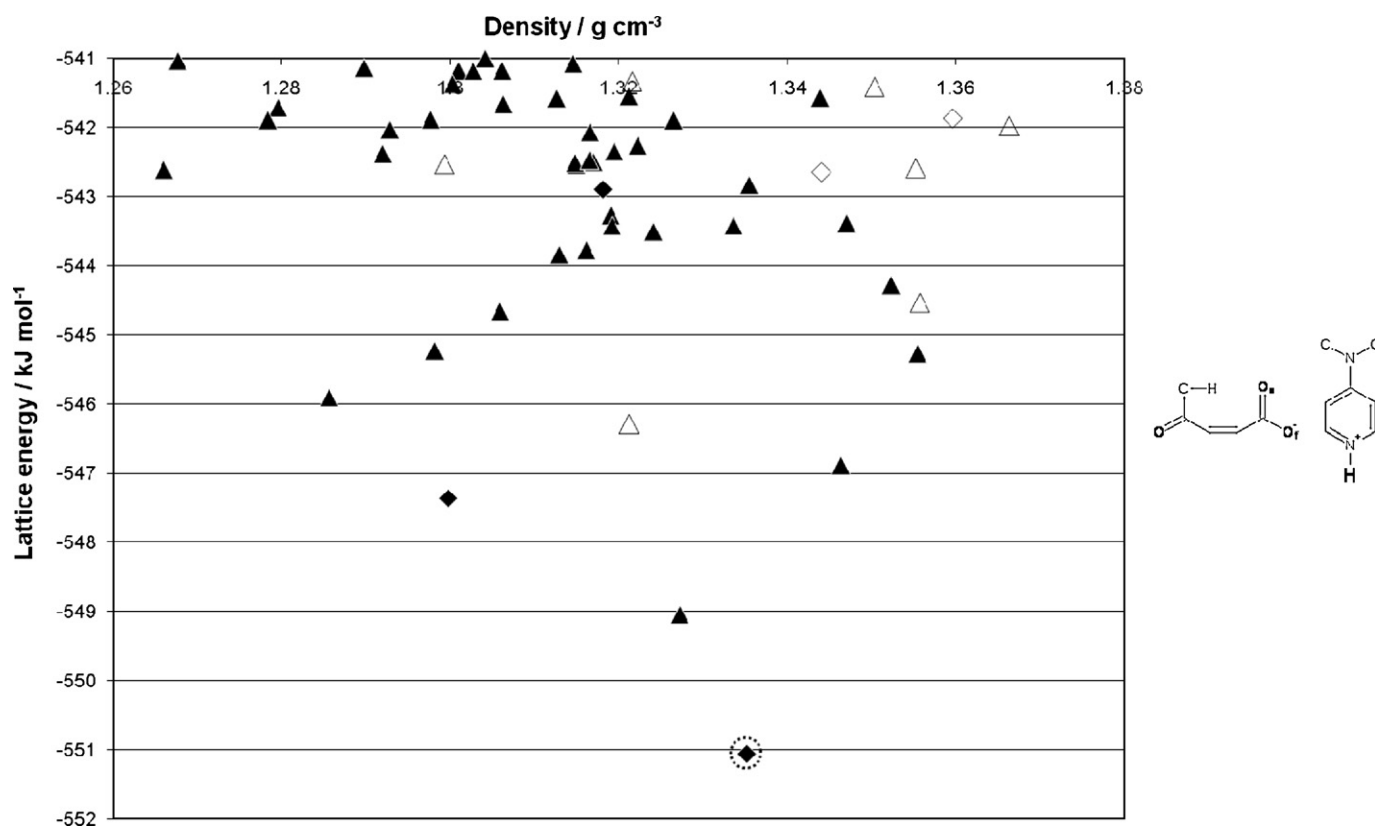


Fig. 6. Lattice energy landscape of the 4-dimethylaminopyridinium maleate salt, with each point representing a crystal structure classified by the graph set of the hydrogen bond motif. Solid diamonds denote the $R_2^2(7)$ motif involving O_r and open diamonds denote the $D_1^1(2)$ motif involving O_r . Solid triangles denote the $R_2^2(7)$ motif involving O_a and open triangles denote the $D_1^1(2)$ motif involving O_a . The large dotted circle denotes the lattice energy minimum corresponding to the experimental structure (GUKVUE).

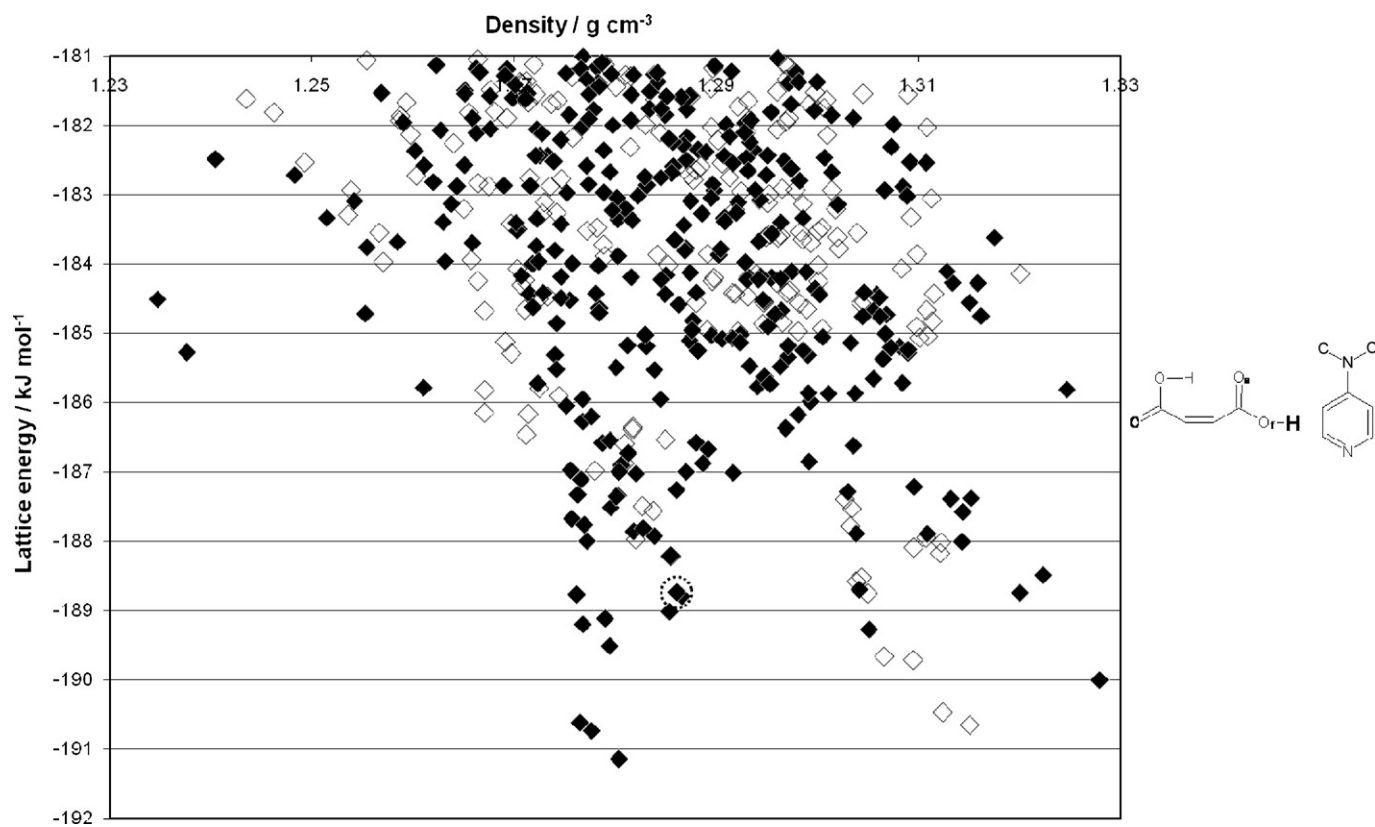


Fig. 7. Lattice energy landscape of the 4-dimethylaminopyridine-maleic acid cocrystal, with each point representing a crystal structure classified by the graph set of the hydrogen bond motif. Solid diamonds denote the $R_2^2(7)$ motif involving O_r and open diamonds denote the $D_1^1(2)$ motif involving O_r . The large dotted circle denotes the lattice energy minimum corresponding to that resulting from the experimental structure (GUKVUE) following repositioning of the acidic proton.

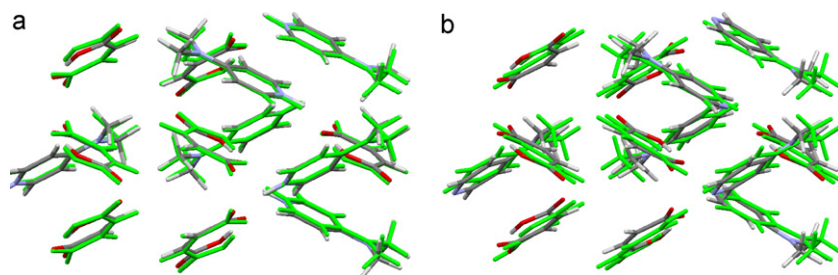


Fig. 8. Overlay of the crystal packings (viewed along the *b*-axis) of GUKVUE (4-dimethylaminopyridinium maleate, colored by element) and (a) the predicted global minimum structure (green) from the salt search (RMSD₁₅ of 0.153 Å) and (b) the predicted global minimum structure (green) from the cocrystal search (RMSD₁₅ of 0.504 Å). (For interpretation of the references to color in this figure legend, the reader is referred to the web version of this article.)

is the second most stable structure found in the search (Fig. 9), only 0.16 kJ mol⁻¹ above the global minimum structure. In the crystal energy landscape of the salt, the minor salt component of **IYUPEX** is ranked 11th in stability, 6.85 kJ mol⁻¹ less stable than the global minimum structure (Fig. 10). The crystal structure is reproduced less well when modelled as a salt, with an RMSD₁₅ of 0.475 Å.

Both acid–base and acid–acid hydrogen bonds occur in all low energy crystal structures, giving a range of motifs defined in Scheme 3 by the overall packing and acid–acid hydrogen bonding motif, and subdivided by the acid–base hydrogen bonding. There are some motifs that appear on both crystal energy landscapes within the 10 kJ mol⁻¹ illustrated in Figs. 9 and 10, but also some motifs that only occur as salts or as cocrystals (Scheme 3) which are relatively stable. Most of the structures with the same hydrogen bonding motif as salt or cocrystal differ significantly in the relative positions of the molecular units: only 5 salts had a cocrystal

structure where all 15 molecules in the coordination sphere could be overlaid in the Crystal Packing Similarity Analysis. Of these 5, the experimental **IYUPEX** structure has by far the best match in RMSD₁₅ and simulated powder patterns between the salt and cocrystal structures. Thus, the limited structural changes induced by proton re-positioning make **IYUPEX** the most likely candidate for disorder in the proton position, given that the relatively small ΔpK_a of the acid–base pair allows for this possibility.

The most stable structures on the cocrystal lattice energy landscape (Fig. 9) are the Column 1 hydrogen bonding motif of **IYUPEX** and some structures based on the R₂²(8) carboxylic acid dimer motif (Scheme 3). On the salt energy landscape, there are three motifs that produce structures that are more stable than **IYUPEX** which correspond to very unstable structures if the proton is transferred to give a cocrystal. For example, the most stable Ribbon Motif 2 structure has the N_{arom}⁺–H donor hydrogen bonded to the *anti*

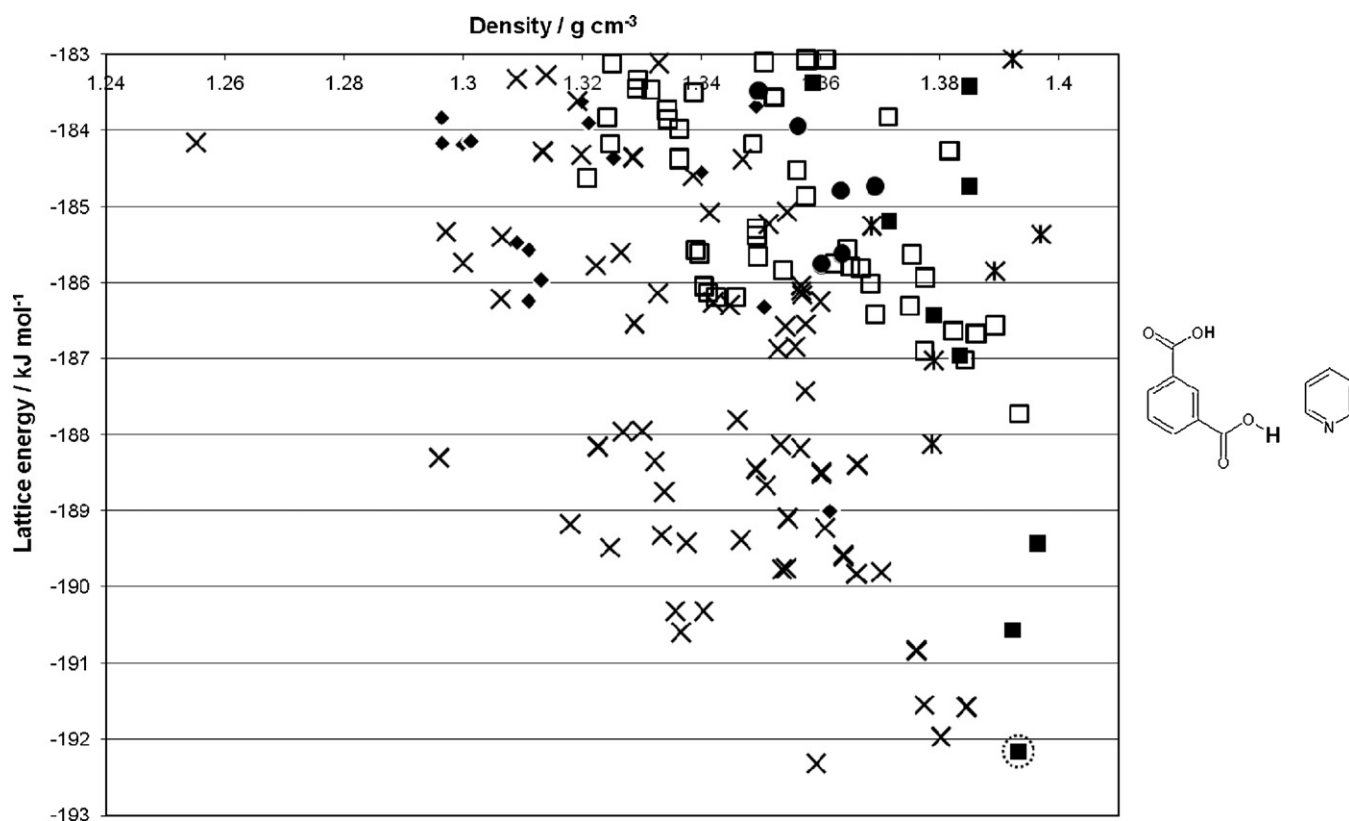


Fig. 9. Lattice energy landscape of the pyridine-isophthalic acid cocrystal, with each point representing a crystal structure classified by the graph set of the hydrogen bond motif (Scheme 3 illustrates these motifs). Solid squares denote crystal structures which exhibit Column 1 hydrogen bonding, solid diamonds denote Column 2 hydrogen bonding, solid circles denote Ribbon 1 hydrogen bonding, open squares denote Catemer hydrogen bonding, crosses denote Dimer hydrogen bonding and stars denote Ring hydrogen bonding. The large dotted circle denotes the lattice energy minimum corresponding to the pyridine-isophthalic cocrystal which forms the major component (58%) of the disordered crystal (**IYUPEX**).

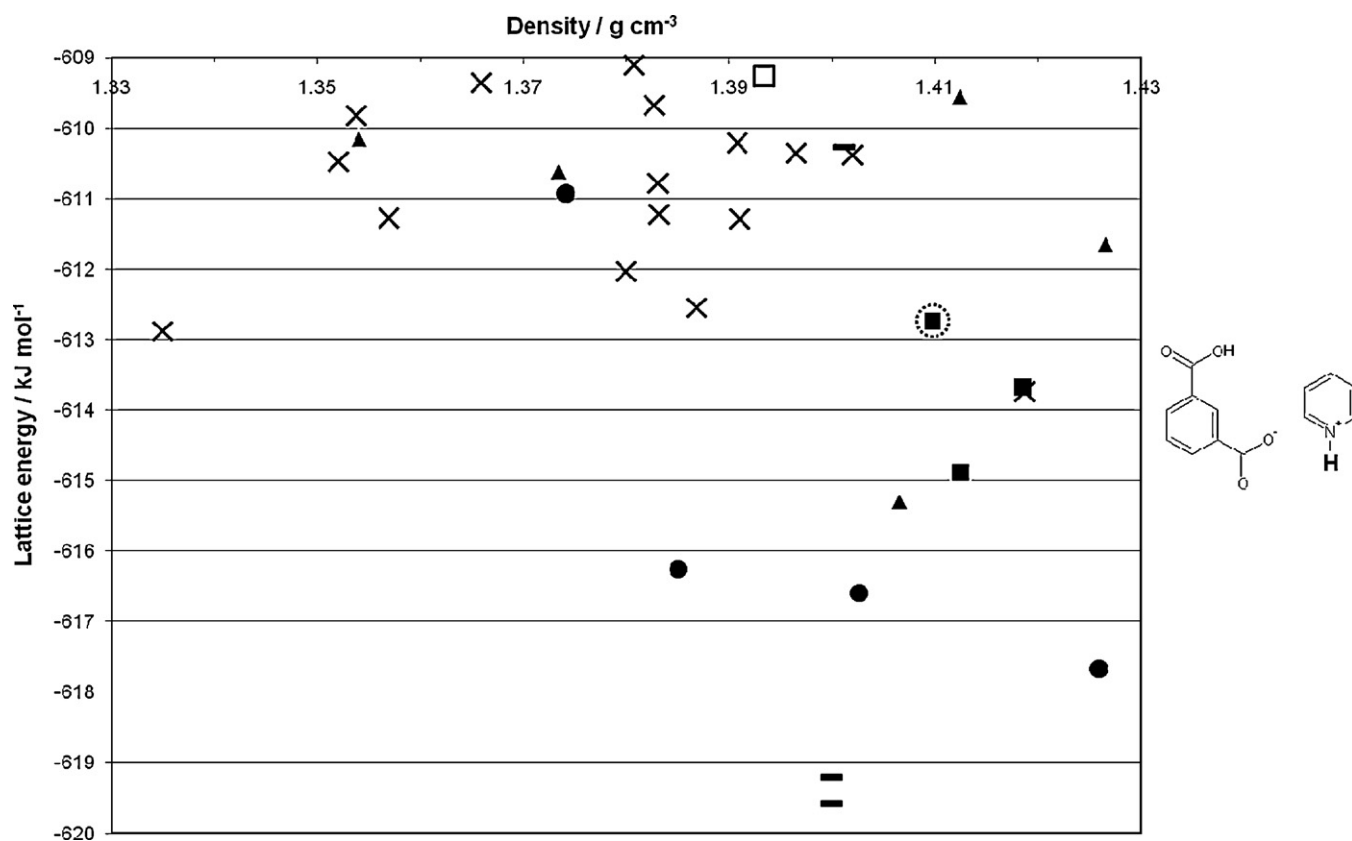


Fig. 10. Lattice energy landscape of the pyridinium isophthalate salt, with each point representing a crystal structure classified by the graph set of the hydrogen bond motif (Scheme 3 illustrates these motifs). Solid squares denote crystal structures which exhibit Column 1 hydrogen bonding, solid circles denote Ribbon 1 hydrogen bonding, bars denote Ribbon 2 hydrogen bonding, solid triangles denote Ribbon 3 hydrogen bonding, open squares denote Catemer hydrogen bonding and crosses denote Dimer hydrogen bonding. The large dotted circle denotes the lattice energy minimum corresponding to the pyridinium isophthalate salt which forms the minor component (42%) of the disordered crystal (IYUPEX).

lone pair on a carboxylate oxygen, a motif not seen in the cocrystal energy landscape. The stability of salt structures with the Ribbon 1, 2 or 3 motifs (Scheme 3) could be overestimated because their hydrogen bond geometries are unlikely to have been sampled in the neutral molecule structures used to fit and validate the model potential. In this case, the observed structure is amongst the most favourable of the salt structures. There are only 3 low energy salt structures (within 8 kJ mol^{-1} of the global minimum) which are similarly favourable as cocrystals after proton re-positioning and all of these are based on the Column 1 packing of **IYUPEX**. The relative energy of these three packings of the Column 1 motif depends on whether the system is modelled as a salt or cocrystal, with **IYUPEX** being the least stable as a salt but the most stable as a cocrystal. Thus the experimental structure **IYUPEX** also stands out as being an energetically favoured structure on both the cocrystal and salt energy landscapes.

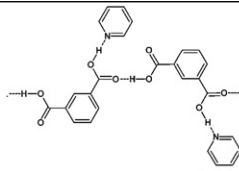
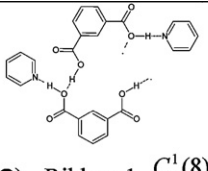
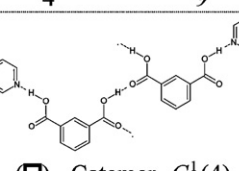
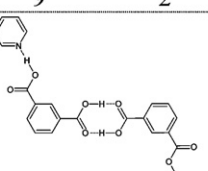
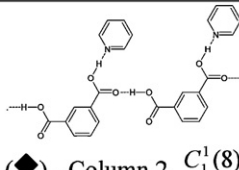
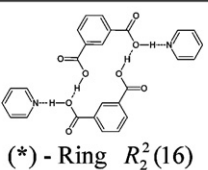
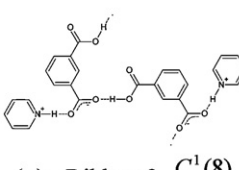
4. Discussion

This paper demonstrates successful searches for the crystal structures of three multi-component crystals, in that the experimental structures were located at or near the global minimum in lattice energy. This shows the ability to suggest likely crystal packings for this type of molecule. It also reveals that there are alternative packings that are competitive in energy. The calculations are not of sufficient accuracy to confirm that the most thermodynamically stable form has been obtained, let alone eliminate the possibility of polymorphism. Thermal effects have been ignored, the structures have not been refined to allow for small conformational changes in response to the crystal pack-

ing (which could be performed at considerable computational expense (Karamertzanis et al., 2009)), and the models for the intermolecular forces are not sufficiently accurate. The novel cocrystal of 4-cyanopyridine-4-fluorobenzoic acid (1:1) should be better modelled by improving the model for the intermolecular interactions of fluorine and cyanide groups. The modelling of the salt structures also neglects the polarization of the charge density by the stronger fields in the crystal environment. The small energy differences between different structures therefore imply that sufficiently accurate calculations of the crystal energy landscape for confident prediction of salt or cocrystal structures will be extremely demanding of computational resources in the foreseeable future.

The successful prediction of the known structures as sufficiently low in energy gives confidence that the lattice energy landscapes are qualitatively meaningful. The calculations demonstrate that there are often a surprising number of ways that the molecular units can form close packed crystal structures with plausible hydrogen bonding motifs which are thermodynamically competitive. Although all the structures contain either the neutral or ionic form of the carboxylic acid–pyridine hydrogen bond, as might have been expected from surveys of the Cambridge Structural Database (Shattock et al., 2008), the motif is often of the $D_1^1(2)$ form, showing the variety of compromises between the other intermolecular interactions and the C–H...O interaction that is often used to define the synthon (Desiraju, 2010).

As with single component lattice energy landscapes, both types considered here have a small number of particularly energetically favourable structures that are clearly separated from a larger number of unfavourable ones. For the salts, this cut-off is about

| | | |
|---|--|---|
| $\text{COO}^- \cdots \text{HN}_{\text{arom}}^+$ Salt $\text{COOH} \cdots \text{N}_{\text{arom}}$ Cocrystal |  (■) - Column 1 $C_1^1(8)$ $R_2^2(7)$ $D_1^1(2)$ 0 3 4 9 |  (●) - Ribbon 1 $C_1^1(8)$ $R_2^2(7)$ $D_1^1(2)$ 4 0 9 2 |
| |  (□) - Catemer $C_1^1(4)$ $R_2^2(7)$ $D_1^1(2)$ 0 1 39 22 |  (×) - Dimer $R_2^2(8)$ $R_2^2(7)$ $D_1^1(2)$ 5 11 81 42 |
| $\text{COO}^- \cdots \text{HN}_{\text{arom}}^+$ Salt $\text{COOH} \cdots \text{N}_{\text{arom}}$ Cocrystal |  (◆) - Column 2 $C_1^1(8)$ $R_2^2(7)$ $D_1^1(2)$ 0 18 |  (*) - Ring $R_2^2(16)$ $R_2^2(7)$ $D_1^1(2)$ 3 4 |
| | $\text{COOH} \cdots \text{N}_{\text{arom}}$ Cocrystal |  (-) - Ribbon 2 $C_1^1(8)$ $R_2^2(7)$ $D_1^1(2)$ 0 3 |

Scheme 3. The hydrogen bond motifs found in the lattice energy landscapes of the salt and cocrystal molecular structures of pyridine-isophthalic acid and pyridinium isophthalate. The numbers of structures within 10 kJ mol^{-1} of the global minimum, i.e. on Figs. 9 and 10, are given for each motif, and the motif key is given in parentheses. For the motifs that are common to the salt and cocrystal energy landscapes (Column 1, Ribbon 1, Catemer and Dimer), the molecular structure of the cocrystal is used for illustration.

8 kJ mol^{-1} above the global minimum (Figs. 5, 6 and 10) while for the cocrystals it is nearer to 5 kJ mol^{-1} (Figs. 4, 7 and 9). The difference in the energy scale when comparing the salt and cocrystal landscape for the same system can be attributed to the stronger ionic hydrogen bonding in the salts, which compensates for the proton transfer energy. However, the salt and cocrystal energy landscapes are not related by a simple scaling, as different types of hydrogen bonding motifs give rise to the most energetically favoured structures. It is quite unusual for the same close packing of the ions or molecules to be energetically favourable for both the salt and cocrystal. Even for the cocrystal, **I**, which was specifically chosen to have the idealized carboxylic acid–pyridine synthon, which is sterically similar in both the ionized and neutral forms, the most favourable salt structures do not correspond to the most favourable cocrystals (or vice versa). The non-equivalence of the carboxylate oxygen atoms (O_a and O_f) in maleic acid results in

most of the favourable salt structures (excluding the experimental one **GUKVUE**) hydrogen bonding to the carboxylate oxygen atom that could not be the donor in the cocrystal. The introduction of competing hydrogen bonding interactions, as in **IYUPEX**, results in some distinct and some common hydrogen bond motifs, but only structures based on the experimental Column 1 motif and structures based on a Dimer are favourable in both landscapes. Thus, whether a multi-component crystal of given stoichiometry is modelled as a salt or a cocrystal makes a major difference to the most thermodynamically favourable packings. The differences in crystallization behaviour can be even more extreme: an analysis of over eighty crystals synthesized from equimolar amounts of carboxylic acids and *N*-heterocycles (Aakeroy et al., 2007) showed that salts quite frequently crystallize as solvates or with unexpected stoichiometries, whereas this was rare amongst the cocrystals.

Clearly in some instances it is artificial to differentiate between a cocrystal and a salt (Desiraju, 2010) as there are many illustrations of the salt: cocrystal continuum (Childs et al., 2007) for acid–base complexes with similar pK_a values. The pyridine-isophthalic acid system is the only one of the three systems in our work where it is impossible to tell whether a salt, cocrystal or proton disordered form would be possible based on the relative pK_a values (5.14 for pyridine, 3.46 and 4.46 for isophthalic acid) (Brown, 1955; Perrin, 1965). Surprisingly, the structurally matched salt and cocrystal are both energetically favourable. Both a small difference in pK_a and energetically similar structures are required to experimentally observe proton disorder. Periodic electronic structure calculations have confirmed that the variation of lattice energy with proton position is far smaller in **IYUPEX** than for related systems that are ordered salts or cocrystals (Mohamed et al., 2009). Such electronic structure calculations can help assign proton positions when solving structures from powder X-ray data (Florence et al., 2009). We note that this may well be helpful, as for all three systems the similarity index for the simulated powder patterns when modelled as a salt or as a cocrystal are all around the borderline for distinguishing between polymorphs and redeterminations of the same structure (van de Streek and Motherwell, 2005). In cases of small ΔpK_a , the results for pyridine-isophthalic acid and pyridinium isophthalate suggest that testing whether the same structure is low in energy on both the salt and cocrystal energy landscapes may be diagnostic of the possibility of a proton-disordered structure. Thus, it seems that a range of calculations may complement experimental studies combining techniques such as infrared-spectroscopy, neutron and X-ray diffraction (Wilson et al., 2006), solid state NMR (Li et al., 2006) and X-ray photoelectron spectroscopy (Stevens et al., 2010a), to determine the proton position in the salt: cocrystal continuum. The ability to characterize systems where the ionization state is influenced by the crystal structure will encourage solid form screening with a wider variety of potential counterions and guest molecules, with the likelihood that this will yield a wider array of solid forms with potentially useful physical properties (Childs et al., 2007).

5. Conclusions

The experimental structures of a salt, cocrystal and disordered system have been found to be amongst the most energetically favourable lattice energy minima in an extensive CrystalPredictor search covering 14 space groups, which generated about a quarter of a million structures. The results are consistent with these being the most thermodynamically stable structures and only forms currently detected in manual crystallization screens. However, the energy differences between the energetically favourable structures are sufficiently small, relative to the approximations in the calculations, that these structures could not be predicted with any confidence.

The lattice energy landscapes show that there are a wide range of different types of crystal structure that are low in energy. Although the experimental structures are amongst the most favourable (i.e. have a lattice energy within 9 kJ mol^{-1} of the most stable) whether modelled as a salt or cocrystal, the acidic proton position generally has a significant effect on the relative energy ordering of different structures, even for a structure that contains an isolated carboxylic acid–pyridine heterosynthon. Hence, when the pK_a difference is insufficient for confident assignment of the acidic proton position, the structure adopted will determine whether a salt, cocrystal or proton disordered crystal is formed. Although the calculation of realistic lattice energy landscapes is now possible for salts and cocrystals, predicting these crystal structures is still a major challenge to computational chemistry and our understanding of the factors that control crystallization.

Acknowledgements

We acknowledge financial support from the EPSRC Basic Technology program (EP/F03573X/1) for the Control and Prediction of the Organic Solid State (www.cposs.org.uk). The computed crystal structures can be provided on request.

Appendix A. Supplementary data

Supplementary data associated with this article can be found, in the online version, at [doi:10.1016/j.ijpharm.2011.03.063](https://doi.org/10.1016/j.ijpharm.2011.03.063).

References

- Aakeroy, C.B., Fasulo, M.E., Desper, J., 2007. Cocrystal or salt: does it really matter? *Mol. Pharm.* 4, 317–322.
- Albert, A., Serjeant, E.P., 1984. *The Determination of Ionization Constants: A Laboratory Manual*. Cambridge University Press.
- Allen, F.H., 2002. The Cambridge Structural Database: a quarter of a million crystal structures and rising. *Acta Crystallogr. B* 58, 380–388.
- Allen, F.H., Kennard, O., Watson, D.G., 1987. Tables of bond lengths determined by X-ray and neutron diffraction. Part 1. Bond lengths in organic compounds. *J. Chem. Soc. Perkin Trans. 2*, S1–S19.
- Almarsson, O., Zaworotko, M.J., 2004. Crystal engineering of the composition of pharmaceutical phases. Do pharmaceutical co-crystals represent a new path to improved medicines? *Chem. Commun.* 17, 1889–1896.
- Beyer, T., Price, S.L., 2000. Dimer or catemer? Low-energy crystal packings for small carboxylic acids. *J. Phys. Chem. B* 104, 2647–2655.
- Bhogala, B.R., Basavouju, S., Nangia, A., 2005. Tape and layer structures in cocrystals of some di- and tricarboxylic acids with 4,4'-bipyridines and isonicotinamide. From binary to ternary cocrystals. *CrystEngComm* 7, 551–562.
- Braun, D.E., Karamertzanis, P.G., Arlin, J.B., Florence, A.J., Kahlenberg, V., Tocher, D.A., Griesser, U.J., Price, S.L., 2011. Solid-state forms of beta-resorcylic acid: how exhaustive should a polymorph screen be? *Cryst. Growth Des.* 11, 210–220.
- Breneman, C.M., Wiberg, K.B., 1990. Determining atom-centered monopoles from molecular electrostatic potentials – the need for high sampling density in formamide conformational-analysis. *J. Comput. Chem.* 11, 361–373.
- Brown, H.C., 1955. *Determination of Organic Structures by Physical Methods*. Academic Press, New York.
- Bruker AXS Inc., 2003. SAINT+ Madison, Wisconsin, USA.
- Childs, S.L., Stahly, G.P., Park, A., 2007. The salt-cocrystal continuum: the influence of crystal structure on ionization state. *Mol. Pharm.* 4, 323–338.
- Chisholm, J.A., Motherwell, S., 2005. COMPACT: a program for identifying crystal structure similarity using distances. *J. Appl. Crystallogr.* 38, 228–231.
- Coombs, D.S., Price, S.L., Willock, D.J., Leslie, M., 1996. Role of electrostatic interactions in determining the crystal structures of polar organic molecules. A distributed multipole study. *J. Phys. Chem.* 100, 7352–7360.
- Cox, S.R., Hsu, L.Y., Williams, D.E., 1981. Nonbonded potential function models for crystalline oxohydrocarbons. *Acta Crystallogr. A* 37, 293–301.
- Cruz-Cabeza, A.J., Day, G.M., Jones, W., 2008. Towards prediction of stoichiometry in crystalline multicomponent complexes. *Chem. Eur. J.* 14, 8830–8836.
- Cruz-Cabeza, A.J., Day, G.M., Motherwell, W.D.S., Jones, W., 2006. Prediction and observation of isostructurality induced by solvent incorporation in multicomponent crystals. *J. Am. Chem. Soc.* 128, 14466–14467.
- Dale, S.H., Elsegood, M.R.J., Hemmings, M., Wilkinson, A.L., 2004. The cocrystallisation of pyridine with benzenepolycarboxylic acids: the interplay of strong and weak hydrogen bonding motifs. *CrystEngComm* 6, 207–214.
- Day, G.M., Cooper, T.G., Cruz-Cabeza, A.J., Hejczyk, K.E., Ammon, H.L., Boerrigter, S.X.M., Tan, J., Della Valle, R.G., Venuti, E., Jose, J., Gadre, S.R., Desiraju, G.R., Thakur, T.S., van Eijck, B.P., Facelli, J.C., Bazterra, V.E., Ferraro, M.B., Hofmann, D.W.M., Neumann, M., Leusen, F.J.J., Kendrick, J., Price, S.L., Misquitta, A.J., Karamertzanis, P.G., Welch, G.W.A., Scheraga, H.A., Arnautova, Y.A., Schmidt, M.U., van de Streek, J., Wolf, A., Schweizer, B., 2009. Significant progress in predicting the crystal structures of small organic molecules – a report on the fourth blind test. *Acta Crystallogr. B* 65, 107–125.
- Desiraju, G.R., 2010. Crystal engineering: a brief overview. *J. Chem. Sci.* 122, 667–675.
- Etter, M.C., MacDonald, J.C., Bernstein, J., 1990. Graph-set analysis of hydrogen-bond patterns in organic-crystals. *Acta Crystallogr. B* 46, 256–262.
- Fischer, A., Vaughan, J., Galloway, W.J., 1964. Structure + reactivity in pyridine series. 1. Acid dissociation constants of pyridinium ions. *J. Chem. Soc.* 3591–3596.
- Florence, A.J., Bardin, J., Johnston, B., Shankland, N., Griffin, T.A.N., Shankland, K., 2009. Structure determination from powder data: Mogul and CASTEP. *Z. Kristallogr.* 215–220.
- Frisch, M.J., Trucks, G.W., Schlegel, H.B., Scuseria, G.E., Robb, M.A., Cheeseman, J.R., Montgomery, J., Vreven, T., Kudin, K.N., Burant, J.C., Millam, J.M., Iyengar, S.S., Tomasi, J., Barone, V., Mennucci, B., Cossi, M., Scalmani, G., Rega, N., Petersson, G.A., Nakatsuji, H., Hada, M., Ehara, M., Toyota, K., Fukuda, R., Hasegawa, J., Ishida, M., Nakajima, T., Honda, Y., Kitao, O., Nakai, H., Klene, M., Li, X., Knox, J.E., Hratchian, H.P., Cross, J.B., Bakken, V., Adamo, C., Jaramillo, J., Gomperts, R., Stratmann, R.E., Yazyev, O., Austin, A.J., Cammi, R., Pomelli, C., Ochterski, J., Ayala, P.Y., Morokuma, K., Voth, G.A., Salvador, P., Dannenberg, J.J., Zakrzewski, V.G., Dapprich, S., Daniels, A.D., Strain, M.C., Farkas, O., Malick, D.K., Rabuck,

- A.D., Raghavachari, K., Foresman, J.B., Ortiz, J.V., Cui, Q., Baboul, A.G., Clifford, S., Cioslowski, J., Stefanov, B.B., Liu, G., Liashenko, A., Piskorz, P., Komaromi, I., Martin, R.L., Fox, D.J., Keith, T., Al Laham, M.A., Peng, C.Y., Nanayakkara, A., Challacombe, M., Gill, P.M.W., Johnson, B., Chen, W., Wong, M.W., Gonzalez, C., Pople, J.A., 2003. Gaussian 03. Gaussian Inc, Wallingford, CT.
- Frisic, T., Jones, W., 2009. Recent advances in understanding the mechanism of cocrystal formation via grinding. *Cryst. Growth Des.* 9, 1621–1637.
- Habgood, M., Deij, M.A., Mazurek, J., Price, S.L., ter Horst, J.H., 2010. Carbamazepine co-crystallization with pyridine carboxamides: rationalization by complementary phase diagrams and crystal energy landscapes. *Cryst. Growth Des.* 10, 903–912.
- Habgood, M., Price, S.L., 2010. Isomers, conformers, and cocrystal stoichiometry: insights from the crystal energy landscapes of caffeine with the hydroxybenzoic acids. *Cryst. Growth Des.* 10, 3263–3272.
- Issa, N., Karamertzanis, P.G., Welch, G.W.A., Price, S.L., 2009. Can the formation of pharmaceutical cocrystals be computationally predicted? I. Comparison of lattice energies. *Cryst. Growth Des.* 9, 442–453.
- Johnson, S.L., Rumon, K.A., 2008. Infrared spectra of solid 1:1 pyridine–benzoic acid complexes; the nature of the hydrogen bond as a function of the acid–base levels in the complex. *J. Phys. Chem.* 69, 74–86.
- Karamertzanis, P.G., Anandamanoharan, P.R., Fernandes, P., Cains, P.W., Vickers, M., Tocher, D.A., Florence, A.J., Price, S.L., 2007. Toward the computational design of diastereomeric resolving agents: an experimental and computational study of 1-phenylethylammonium-2-phenylacetate derivatives. *J. Phys. Chem. B* 111, 5326–5336.
- Karamertzanis, P.G., Kazantsev, A.V., Issa, N., Welch, G.W.A., Adjiman, C.S., Pantelides, C.C., Price, S.L., 2009. Can the formation of pharmaceutical co-crystals be computationally predicted? II. Crystal structure prediction. *J. Chem. Theory Comput.* 5, 1432–1448.
- Karamertzanis, P.G., Pantelides, C.C., 2005. Ab initio crystal structure prediction – I. Rigid molecules. *J. Comput. Chem.* 26, 304–324.
- Karki, S., Friscic, T., Jones, W., Motherwell, W.D.S., 2007. Screening for pharmaceutical cocrystal hydrates via neat and liquid-assisted grinding. *Mol. Pharm.* 4, 347–354.
- Li, Z.J., Abramov, Y., Bordner, J., Leonard, N.J., Medek, A., Trask, A.V., 2006. Solid-state acid–base interactions in complexes of heterocyclic bases with dicarboxylic acids: crystallography, hydrogen bond analysis, and ^{15}N NMR spectroscopy. *J. Am. Chem. Soc.* 128, 8199–8210.
- Macrae, C.F., Bruno, I.J., Chisholm, J.A., Edgington, P.R., McCabe, P., Pidcock, E., Rodriguez-Monge, L., Taylor, R., van de Streek, J., Wood, P.A., 2008. Mercury CSD 2.0 – new features for the visualization and investigation of crystal structures. *J. Appl. Crystallogr.* 41, 466–470.
- Macrae, C.F., Edgington, P.R., McCabe, P., Pidcock, E., Shields, G.P., Taylor, R., Towler, M., De Streek, J., 2006. Mercury: visualization and analysis of crystal structures. *J. Appl. Crystallogr.* 39, 453–457.
- Mohamed, S., Tocher, D.A., Vickers, M., Karamertzanis, P.G., Price, S.L., 2009. Salt or cocrystal? A new series of crystal structures formed from simple pyridines and carboxylic acids. *Cryst. Growth Des.* 9, 2881–2889.
- Perrin, D.D., 1965. Dissociation Constants of Organic Bases in Aqueous Solution. Butterworths, London.
- Polito, M., D’Oria, E., Maini, L., Karamertzanis, P.G., Grepioni, F., Braga, D., Price, S.L., 2008. The crystal structures of chloro and methyl ortho-benzoic acids and their co-crystal: rationalizing similarities and differences. *CrystEngComm* 10, 1848–1854.
- Price, S.L., 2004. The computational prediction of pharmaceutical crystal structures and polymorphism. *Adv. Drug Deliv. Rev.* 56, 301–319.
- Price, S.L., 2009. Computed crystal energy landscapes for understanding and predicting organic crystal structures and polymorphism. *Acc. Chem. Res.* 42, 117–126.
- Price, S.L., Leslie, M., Welch, G.W.A., Habgood, M., Price, L.S., Karamertzanis, P.G., Day, G.M., 2010. Modelling organic crystal structures using distributed multipole and polarizability-based model intermolecular potentials. *Phys. Chem. Chem. Phys.* 12, 8478–8490.
- Sarma, B., Nath, N.K., Bhogala, B.R., Nangia, A., 2009. Synthon competition and cooperation in molecular salts of hydroxybenzoic acids and aminopyridines. *Cryst. Growth Des.* 9, 1546–1557.
- Shattock, T.R., Arora, K.K., Vishweshwar, P., Zaworotko, M.J., 2008. Hierarchy of supramolecular synthons: persistent carboxylic acid–pyridine hydrogen bonds in cocrystals that also contain a hydroxyl moiety. *Cryst. Growth Des.* 8, 4533–4545.
- Sheldrick, G.M., 1997a. SHELXL97 Göttingen. University of Göttingen, Germany.
- Sheldrick, G.M., 1997b. SHELXS97 Göttingen. University of Göttingen, Germany.
- Sheldrick, G.M., 2001. SADABS (Version 2.03) Program for Bruker Area Detector Absorption Correction Göttingen. University of Göttingen, Germany.
- Stevens, J.S., Byard, S.J., Schroeder, S.L.M., 2010a. Characterization of proton transfer in co-crystals by X-ray photoelectron spectroscopy (XPS). *Cryst. Growth Des.* 10, 1435–1442.
- Stevens, J.S., Byard, S.J., Schroeder, S.L.M., 2010b. Salt or co-crystal? Determination of protonation state by X-ray photoelectron spectroscopy (XPS). *J. Pharm. Sci.* 99, 4453–4457.
- Stone, A.J., 2005. Distributed multipole analysis: stability for large basis sets. *J. Chem. Theory Comput.* 1, 1128–1132.
- van de Streek, J., Motherwell, S., 2005. Searching the Cambridge Structural Database for polymorphs. *Acta Crystallogr. B* 61, 504–510.
- van de Streek, J., Neumann, M.A., Perrin, M.A., 2010. Validation of dispersion-corrected density functional theory calculations for the crystal structure prediction of molecular salts: a crystal structure prediction study of pyridinium chloride. *CrystEngComm* 12, 3827–3833.
- Verwer, P., Leusen, F.J.J., 1998. Computer simulation to predict possible polymorphs. In: Lipkowitz, K.B., Boyd, D.B. (Eds.), *Reviews in Computational Chemistry*, vol. 12. John Wiley and Sons Inc, New York, pp. 327–365.
- Williams, D.E., Cox, S.R., 1984. Nonbonded potentials for azahydrocarbons: the importance of the coulombic interaction. *Acta Crystallogr. B* 40, 404–417.
- Williams, D.E., Houpt, D.J., 1986. Fluorine nonbonded potential parameters derived from crystalline perfluorocarbons. *Acta Crystallogr. B* 42, 286–295.
- Wilson, C.C., Xu, X.L., Florence, A.J., Shankland, N., 2006. Temperature dependence of proton transfer in 4-chlorobenzoic acid. *New J. Chem.* 30, 979–981.